Research

Photocatalytic activity of Fe_3O_4–Fe_2O_3 particles supported on mordenite under visible light exposure for methylene blue degradation

Raúl Avilés-Monreal[1] · Hugo A. Borbón-Nuñez[1,2] · M. H. Farías[1] · Felipe Castillón-Barraza[1]

Received: 29 August 2023 / Accepted: 16 November 2023
Published online: 20 December 2023

Abstract

Dyes pollution is a serious environmental problem and heterogeneous catalysis has been proposed as a remediation method. In this study, a set of catalysts of synthetic mordenite with iron oxides was synthesized by a simple chemical co-precipitation method assisted by subsequent thermal treatment with an oxidation process. Physicochemical characterization of prepared materials was performed by a variety of techniques, including XRD, SEM, EDS, S_{BET}, UV–Vis DR, and XPS. Photocatalytic methylene blue (MB) degradation by the synthesized catalyst was evaluated with visible light excitation. From the studied set of catalysts, the sample prepared with a thermal treatment at 100 °C in air atmosphere for 3 h was capable of degrading ~ 90% of MB after 120 min with visible light of λ = 420 nm exposition and a small portion of H_2O_2 added. The catalyst used three processes to degrade MB: (1) adsorption of organic residues in the mordenite matrix support for electrostatic interactions, (2) photocatalysis heterogeneous reaction with visible light and (3) Fenton reaction catalyst with a small portion to H_2O_2 by Fe_3O_4–Fe_2O_3 presence. The catalytic efficiency to dye degradation was improved by a simple and economical thermal treatment without changing reaction conditions like pH, temperature, dose, or other. Studied mordenite iron oxide catalysts can be retrieved and reused at least five times without noticeable degradation, taking advantage of their magnetic properties. These catalysts could be proposed an economical, simple, and non-toxic alternative for eliminating organic dye pollution using visible light or solar irradiation in wastewater remediation related to textile, food, and pharmaceutical industries.

Highlights

- The Fe_3O_4–Fe_2O_3 supported on mordenite catalyst was synthesized for the first time by a simple and cost-effective chemical method.
- Elimination of methylene blue using the catalyst synthesized was accomplished with visible light excitation.
- Reuse of the catalyst for the photodegradation process of dyes from aqueous solution was achieved by magnetic retrieval.
- It was possible to improve the photocatalytic efficiency by facile and economical thermal treatments without changing the pH, temperature, dose, or other conditions.

Keywords Photocatalysis · Dye degradation · Zeolite · Fe_3O_4 · Methylene blue

✉ Felipe Castillón-Barraza, fcastillon@ens.cnyn.unam.mx | [1]Centro de Nanociencias y Nanotecnología, Universidad Nacional Autónoma de México, Km 107 Carretera Tijuana-Ensenada s/n, Ensenada, B.C. C.P. 22800, México. [2]CONAHCYT-Centro de Nanociencias y Nanotecnología, UNAM, Km 107 Carretera Tijuana-Ensenada s/n, Ensenada, B.C C.P. 22800, México.

1 Introduction

Nowadays, environmental problems due to water pollution have recently drawn much attention from researchers. One of the main pollution sources comes from wastewater containing dyes discharged from textiles, foodstuffs, and leather industries [1]. The presence of colored organic compounds in dye-bearing effluents generally reduces sunlight transmission, affecting photosynthesis and harming aquatic ecosystems [2–5]. Besides, dyes are complex structures with high molecular weight, which are soluble in water, degradation-resistant, potentially carcinogenic, and mutagenic. Thus, the development of easy, cheap, and green methods for water pollution treatment has been a priority area in the field of environmental sciences [6, 7].

Methylene blue (MB) is an aromatic heterocyclic basic dye. MB is a well-known cationic and primary thiazine dye, having λ_{max} of 664 nm absorbance. It is highly water-soluble and very stable at room temperature. It is a persistent pollution that has many potential applications in the textile, pharmaceutical, paper, dyeing, printing, paint, medicine, and food industries [8]. It is the most common dye in the textile industry. Advanced oxidation processes (AOPs) were developed to treat toxic organic pollutants, such as MB, through strong redox processes with specific radicals generated in this process without generating any additional harmful substances. AOPs approaches employed for the photodegradation of MB are ozonation, ultraviolet/H_2O_2 oxidation, electrochemical oxidation/degradation, catalytic oxidation, Fenton reaction, photocatalytic degradation, etc. It is desirable to have more than one mechanism that eliminates the presence of methylene blue. Besides, efficiency of the heterogeneous photocatalyst process depends on variables such as irradiation time, light source, dye concentration, pH, oxidant compounds and radical scavengers [9, 10].

Photocatalysis has emerged as a promising technology way to solve pollution problems. Using photocatalytic processes to remove dyes from such effluents might result in decolorization and complete degradation [11]. Semiconductors, due to large band gap and properties, have been used as photocatalytic material with UV/Visible light and, potentially, the practical application of natural solar light [12]. For example, in 2021 Al-Jemeli et al. reported degradation of anti-inflammatory drugs by solar photocatalysis process [13]. Recently, several authors reported photocatalysis as a possible remediation method for the elimination of organic pollution in water and studied different semiconductor hybrid materials for this application, for example in 2023 Bassim et al. reported a green synthesis of CuO/TiO_2 nanoparticles were obtained using a natural extract for degrading methylene blue with photocatalysis under ultraviolet light irradiation [14]. In 2023, Xin et al. reported synthesis of nanoflowers of Bi/BiOBr applied for NO removal by photocatalysis using visible light irradiation [15]. In 2023, Dawi et al. reported the synthesis of $NiTiO_3$ by hydrothermal method for eliminating CO_2 by photocatalytic reduction to CH_4 and water splitting [16]. However, most authors have used materials based on titanium oxide requiring excitation with ultraviolet light, and the difficulty for retrieving the catalyst. Besides, iron oxides are considered favorable semiconductors for photocatalytic reactions due to their band gap of ~ 2.3 eV and good absorbers of visible light with the possibility to take advantage of solar light, they possess excellent stability, can be recyclable, and are highly available [17]. Iron oxides absorb visible light and generate reactive charge carriers, which can promote chemical reactions by activating the adjacent chemical compounds [18–22]. Iron oxides, as reported by several authors [23–26], are used as catalysts of dye waste degradation through photocatalysis heterogeneous reactions or applying the fenton reaction with hydrogen peroxide and iron cationic species (Fe^{3+} and Fe^{2+}). Furthermore, since iron oxide compounds can be manipulated by a magnetic field, catalysts based on iron oxides can be retrieved and reutilized.

The performance of catalysts can be improved by loading on porous, large surface area supports, such as alumina, porous carbon, zeolites, or graphene oxide [27]. Zeolites are crystalline hydrated aluminosilicates composed of Si (Si^{4+}) tetrahedral structures binding with four oxygen atoms, where a fraction of Si atoms can be substituted for Al atoms (Al^{3+}), forming ionic exchange sites from compensation charges. Si/Al atomic ratio is an important property in zeolites. Normally, lower values are indicative of natural zeolites with major ion exchange capacity and, higher values, for synthetic zeolites with good adsorption properties to organic substances. They possess ordered structures containing one-, two-, or three-dimensional cavities and channels with sizes up to 2 nm, through which a large number of molecules can pass [28–30]. The union and combination of Si, O, and Al atoms form many types of Zeolite structures. An important zeolite is mordenite, with good properties as catalytic support. Mordenite belongs to the pentasil family, which has five membered rings as secondary building units. The mordenite structure is composed of connected 5-membered rings forming a composite building unit "mor" [31]. There are only a few articles related to the photocatalysis of wastewater using mordenite-type Zeolite. Mordenite has high thermal and acid stability and has been used as a catalyst for different reactions. Mordenite has also been used in the adsorptive separation of gas or liquid mixtures and for applications in semiconductors, chemical sensors, and nonlinear optics [32]. Semiconductors supported in zeolites forming

hybrid materials could be more efficient for photocatalysis applications, as has been reported recently by authors for different catalytic chemical reactions, like dye pollution degradation. For example, few authors have used hybrid semiconductor materials supported in zeolites. In 2018, Jorfi et al. evaluated the capability of sono-photocatalytic process for real wastewater over MgO supported by zeolite, with 76% efficiency after 4 h [33]. In 2018, Rahmani-Aliabadi et al. informed the synthesis of FeS and Fe_2S_3 supported onto clinoptilolite nanoparticles via sulfidizing and photocatalytic properties for ciprofloxacin degradation with visible light [34]. In 2020, Padervand et al. reported a photocatalyst based on cerium supported in zeolite used for degrading acetamiprid insecticide with ultraviolet excitation. It was synthesized by coprecipitation method and obtained 82% efficiency of degradation after 180 min under ultraviolet irradiation [35]. In 2022, Torkian et al. reported the synthesis and photocatalytic properties for amoxicillin degradation of silver ion-exchanged natural zeolite/TiO_2 photocatalyst nanocomposite with 35% efficiency after 75 min [36]. Also in 2022, Liu et al. reported MoS_2 with zeolite photocatalysts synthesized by combining ultrasonic and hydrothermal methods and it was used for degrading tetracycline with 87% efficiency [37]. However, to our best knowledge, there is no report using iron oxides/mordenite as an alternative to the common TiO_2 catalyst, applying visible light excitation and taking advantage of magnetic retrieval for reusability of the catalyst.

In this paper, we report the methylene blue photodegradation capabilities under visible light of a catalyst based on Fe_3O_4–Fe_2O_3 particles supported on synthetic mordenite (Si/Al = 20), which was synthesized by a facile co-precipitation method. Besides, photocatalytic efficiency was improved by a simple and economical thermal treatment without changing pH, temperature, dose or other conditions. This catalyst seems promising for dye wastewater treatment remediation with solar radiation, applied to textile, food, and pharmaceutical industries.

2 Materials

The following reagent grade materials were acquired and utilized without modification. $Na(AlO_2)(SiO_2)_x{\cdot}yH_2O$ (Mordenite Si/Al ratio = 20, Zeolyst International, USA); Iron (II) chloride tetrahydrate ($FeCl_2{\cdot}4H_2O$ 98%, Sigma-Aldrich, USA); Iron (III) chloride hexahydrate ($FeCl_3{\cdot}4H_2O$ 97%, Sigma-Aldrich, USA); Sodium hydroxide (NaOH 97% Sigma-Aldrich, USA); and Methylene Blue hydrate ($C_{16}H_{18}ClN_3S{\cdot}xH_2O$ > 95% Sigma-Aldrich, USA). Deionized water (pH ~ 7, $\sigma \leq 5 \times 10^{-6}$ S/m) was also utilized.

3 Methods

Catalyst of Fe_3O_4–Fe_2O_3 supported on mordenite (Fe_3O_4–Fe_2O_3/mordenite) was synthesized by co-precipitation. 4 g of synthetic mordenite was added into 60 ml deionized water under magnetic stirring for 10 min to disperse the precipitate. Then, 0.76 g $FeCl_3$ and 0.28 g $FeCl_2$ (2:1) were added to the solution under magnetic stirring for 30 min. After using 20 ml of NaOH 4 M, the solution was precipitated, and the catalyst was collected by centrifugation at 2500 rpm for 15 min and washed with deionized water. The precipitate was dried in an oven at 50 °C for 24 h [38–43]. Following, the obtained powder was divided into four parts. One part was separated and used without thermal treatment, while the other three parts were subjected to a partial thermal oxidation process at 100 °C, 200 °C and 300 °C for 3 h in air. Fe_3O_4–Fe_2O_3 particles were prepared according to reports [44–46].

Structural properties were studied by X-ray diffraction (XRD) and data was collected using a PhilipsTM X´pert MPD diffractometer with a Cu Kα radiation (λ = 1.54056 Å), operating at room temperature. Morphology was analyzed by scanning electron microscopy (SEM) using a JEOL™ model JSM 5300 system with energy dispersive spectroscopy (EDS) detector Kevex SuperDry II for chemical analysis. All samples were placed on carbon tape for analysis. Surface area analysis and textural properties were estimated with a Micromeritics Vacprep 061 equipment assisted by N_2 adsorption to 77 K. Diffuse reflectance spectra were obtained with a Cary 5000 UV–Vis-NIR spectrophotometer with a scanned wavelength from 800 to 200 nm. X-ray Photoelectron Spectroscopy (XPS) measurements were carried out in a SPECS system equipped with a hemispherical electron analyzer model PHOIBOS 150 WAL and a monochromatic X-ray source, model XRC 1000, using Al Kα line (1486.6 eV) at 200 W. Also, high-resolution spectra were obtained at a pass energy of 20 eV. For simplicity, samples are labeled as follows: pristine mordenite (M), and prepared catalysts, without thermal treatment (MFe), with thermal treatment at 100 °C for 3 h in air atmosphere (MFe100), with thermal treatment at 200 °C for 3 h in air atmosphere (MFe200), and with thermal treatment at 300 °C for 3 h in air atmosphere (MFe300).

Photocatalytic properties were evaluated in a photochemical reactor Rayonet, model RPR 100, equipped with 16 lamps with a wavelength of 420 nm. Catalyst degradation was carried out at constant stirring and 100 mL/min air flow. 250 mL of the solution to 20 ppm of MB with 125 mg of catalyst were added in a cylindrical quartz cell inside the reactor, and the adsorption process was separated to keep the solution in dark condition for 30 min and subsequently photodegradation reaction with visible light excitation for 2 h. A mechanical stirrer was used to achieve

a satisfactory suspension of the photocatalyst and the homogeneity of the reacting mixture. Samples at 15 min intervals were withdrawn. The change of intensity of the absorption peak at 664 nm was monitored by UV–Vis spectroscopy in a Varian Cary® 50 UV–Vis spectrometer. 2.5 ml H_2O_2 (30%) was added to the solution photodegradation mentioned for evaluating MB elimination by the Fenton reaction catalyzed by the Fe_3O_4–Fe_2O_3 supported on mordenite samples.

4 Results and discussion

4.1 X-Ray diffraction

Crystallinity and thermal stability are important properties of supports used in photodegradation applications. Figure 1 shows XRD patterns of M, MFe, MFe100, MFe200 and MFe300 samples. XRD peaks can be indexed to pure mordenite zeolite orthorhombic structure crystallographic XRD pattern JCPDS 43–0171, without peaks of other chemical agents. Peaks are sharp, indicating high crystallinity. Also, they show a tendency to decrease crystallinity as a function of temperature of treatment. There is broadening of peaks as temperature increases, which could be related to dealumination in the mordenite structure. In addition, the insert on the right side of the figure shows the region of the peak corresponding to (202) plane. Although the signal is relatively weak, Fe_3O_4–Fe_2O_3 supported on mordenite samples show this peak at higher angles in comparison with the pristine mordenite. It is related to the dealumination process because the Si–O bond (1.60 Å) is shorter than the Al–O bond (1.74 Å) in mordenite. The lattice shrinks when the Al species is leached from the zeolite framework, which means the Al species has successfully escaped [47].

4.2 Scanning electron microscopy and elemental analysis

In Fig. 2, SEM images reveal rough structures with aggregated particles of various sizes, lower than 1000 nm. Figure 2b of prepared catalyst without thermal treatment shows a similar structure than Fig. 2a of pristine mordenite, with more homogeneous and smaller particles. This could be due to the incorporation of Fe_3O_4–Fe_2O_3 on mordenite. Images of Figs. 2c–e, corresponding to MFe100, MFe200 and MFe300, show larger size agglomerates, which could be due to sintering and/or dealumination.

To know the chemical composition of the Fe_3O_4–Fe_2O_3 supported on mordenite samples, elemental chemical analysis using EDS was performed on the synthesized catalysts. Results presented in Table 1 show the presence of Al, Si, O, Na and Fe for all synthesized samples with an indication of dealumination process as a function of temperature of the thermal treatment.

Following, to know the Fe distribution in the mordenite support in studied samples, an elemental mapping for the sample of MFe100 was obtained, and results are presented in Fig. 3. Al, Si, O, Na and Fe presence is revealed, with Fe atoms well distributed on the mordenite support. This homogeneous distribution of Fe atoms is very convenient since they are used as the catalytic active center for the photodegradation of contaminants.

4.3 UV–Vis optical diffuse reflectance

Optical properties of materials are related to the electronic structure. The calculated results of diffuse reflectance and

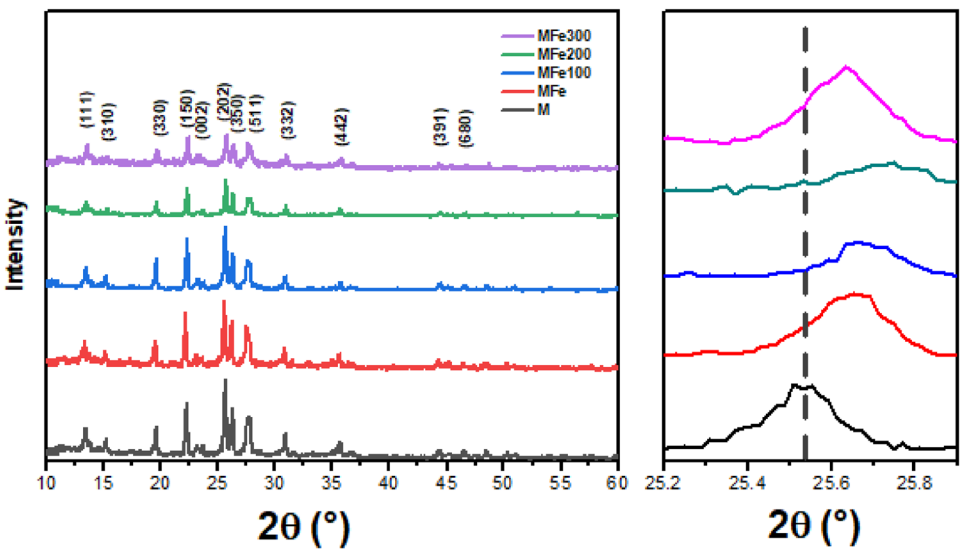

Fig. 1 XRD patterns of Pristine mordenite and Fe_3O_4–Fe_2O_3 supported on mordenite samples

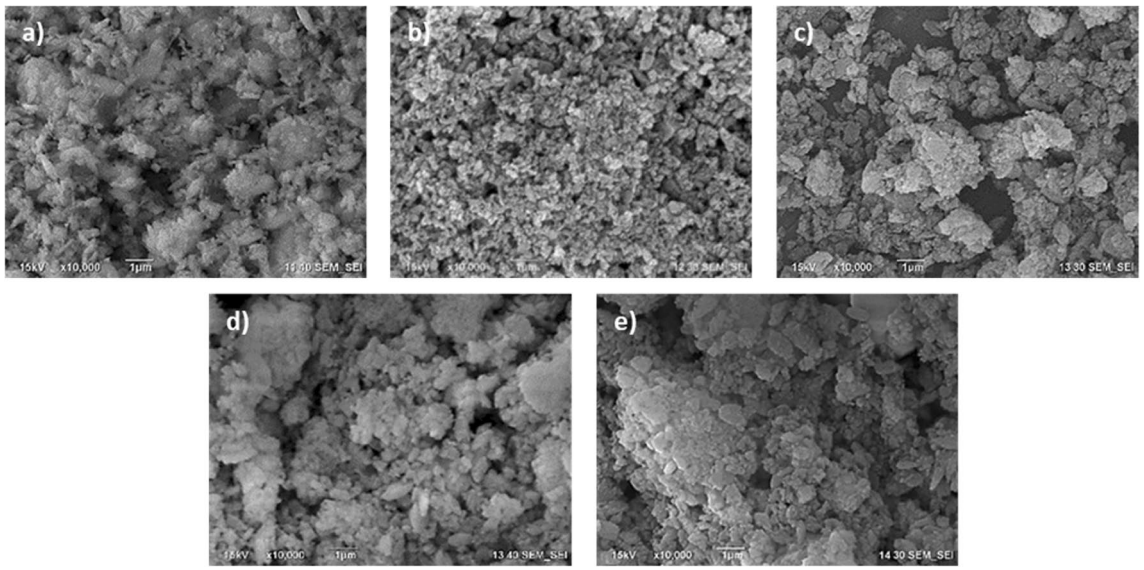

Fig. 2 SEM Images of studied samples. **a** M, **b** MFe, **c** MFe100, **d** MFe200 and **e** MFe300

Table 1 Elemental analysis of Fe_3O_4–Fe_2O_3 supported on mordenite samples

Element	MFe		MFe100		MFe200		MFe300	
	W %	At %	W %	At %	W %	At %	W %	At %
Si	32.4	22.8	32.1	22.7	33.7	23.9	33.2	23.4
Al	4.5	3.7	4.3	3.6	3.4	2.9	3.8	3.2
Na	3.6	3.8	3.8	4.1	3.9	4.2	3.1	3.3
O	54.7	67.9	55.2	68.9	53.5	66.9	34.9	68.2
Fe	4.8	1.8	4.6	1.7	5.5	2.1	5.0	1.9

band gap energy of studied samples are presented in Fig. 4. As shown in Fig. 4a, M sample has high diffuse reflectance for wavelengths > 400 nm, corresponding to visible light. However, mordenite samples with iron oxides present low diffuse reflectance for wavelengths > 400 nm, corresponding to important visible light absorption, from green to violet. Low optical diffuse reflectance for visible light of Fe_3O_4–Fe_2O_3 supported on mordenite samples can be used for photodegradation reaction of contaminants excited by visible light. Direct optical band gap energy (E_g) was estimated for M, MFe, MFe100, MFe200 and MFe300 samples using the equation proposed by Kubelka and Munk in 1931:

$$\frac{K}{S} = \frac{(1-R)}{2R} = F(R)$$

where S, R, K and F are the scattering, reflectance, absorption coefficients, and Kubelka–Munk function, respectively. E_g and the absorption coefficient are related through the Tauc relation [48]:

$$(\alpha h\nu)^n = A(h\nu - E_g)$$

where α is the linear absorption coefficient, ν is light frequency, h is the Planck constant, and A is the proportionality constant. The power of the parenthesis, n, is taken equal to 2 for direct band gap materials. When incident radiation scatters in a perfectly diffuse manner, the absorption coefficient K becomes equal to 2α. In this case, considering constant the scattering coefficient S, concerning wavelength, the Kubelka–Munk function is proportional to the absorption coefficient α. Applying the last equation, we obtain the relation [49]:

$$\left[F(R)h\nu\right]^2 = A(h\nu - E_g)$$

The $\left[F(R)h\nu\right]^2$ vs. $h\nu$ (photon energy) graph is plotted, and the energy band gap of the powder sample can be easily extracted.

The value of E_g for studied samples was obtained by plotting $\left[F(R)h\nu\right]^2$ as function of $h\nu$ (Fig. 4b) and

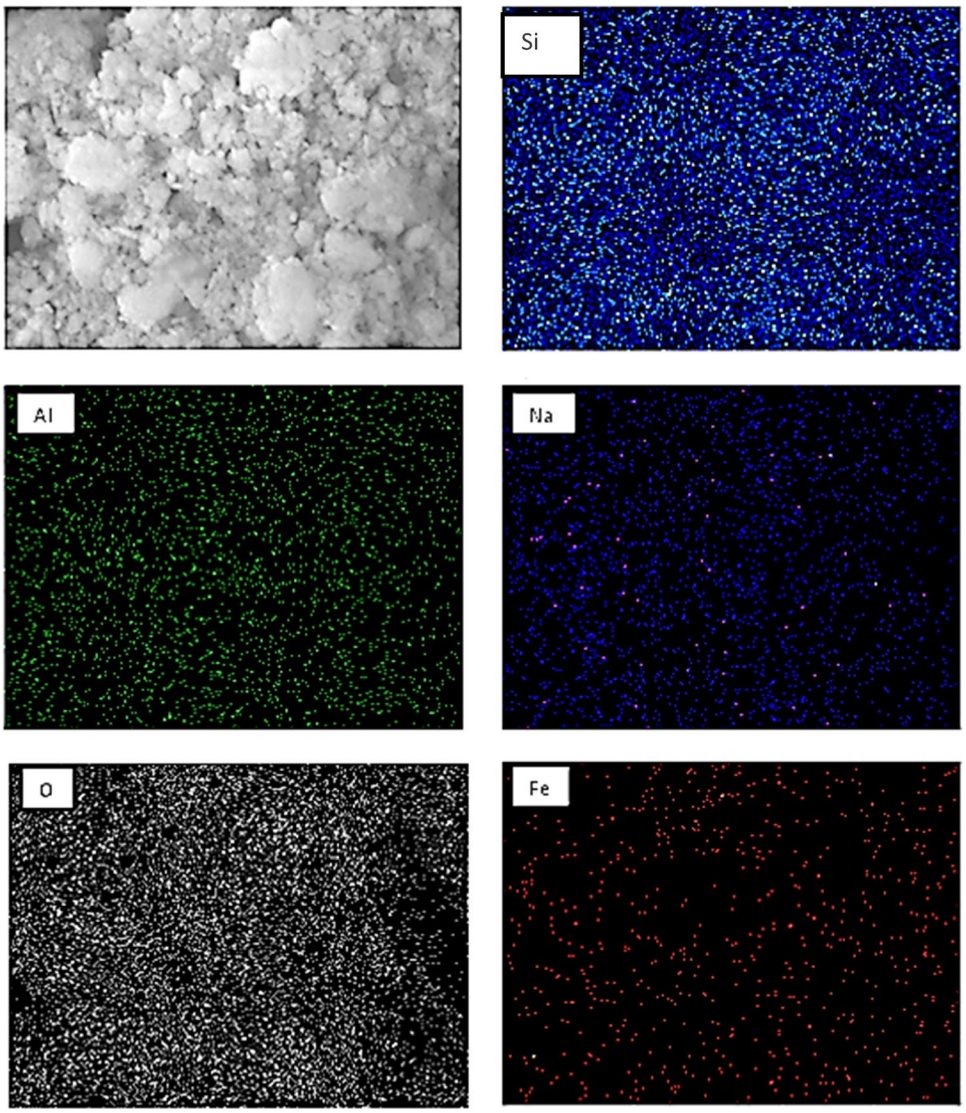

Fig. 3 SEM–EDS elemental mapping of MFe100 sample composition where the first image is the secondary electron image and analogous elemental mapping of the element in the other images

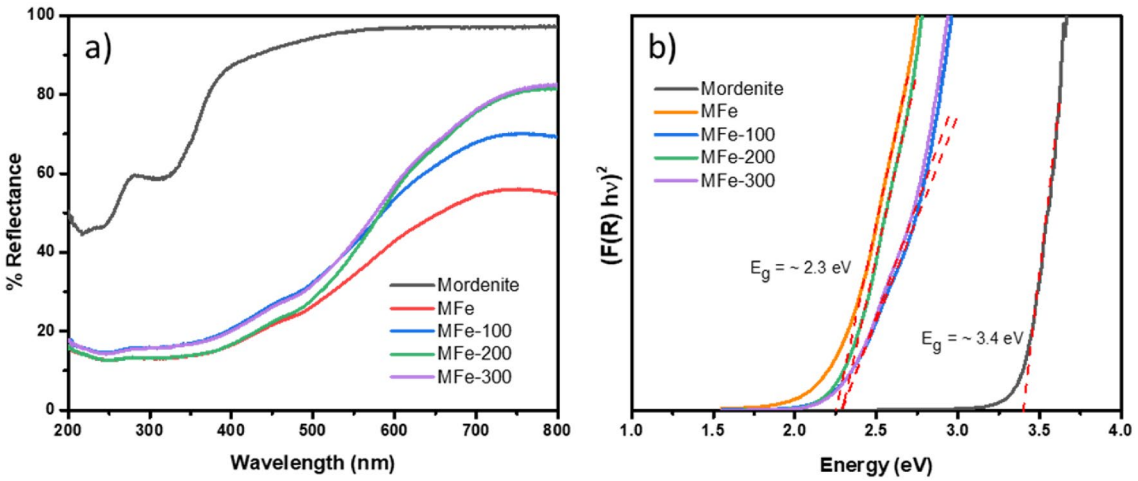

Fig. 4 **a** UV–Vis diffuse reflectance spectra and **b** Band gap estimate by Kubelka–Munk method of, pristine mordenite and Fe_3O_4–Fe_2O_3 supported on mordenite samples

extrapolation of the linear portion of the curve. The obtained results are presented in Fig. 4b. Estimated band gap values for pristine mordenite and Fe_3O_4–Fe_2O_3/mordenite samples with different thermal treatments in air atmosphere are ~ 3.4 eV and ~ 2.25 eV, respectively. These results agree with reports of other authors using iron oxide nanoparticles with different organic modifiers [40] or using iron oxide nanoparticles [39, 50]. Moreover, the band gap energy value estimated for the Fe_3O_4–Fe_2O_3 supported on mordenite samples shows the possibility of promoting the generation of free charge carriers by using visible light, improving the photodegradation process.

4.4 X-ray photoelectron spectroscopy

Survey XPS was obtained to confirm the chemical composition of Fe_3O_4–Fe_2O_3 supported on mordenite samples. Figure 5a shows six signal peaks located at 1072 eV, 103 eV, 532 eV, 75 eV, 285 eV and 712 eV, corresponding to Na 1s, Si 2p, O 1s, Al 2p, C 1s, and Fe $2p_{3/2}$, respectively. Also, high-resolution spectra of the Fe 2p region were obtained for MFe, MFe100, MFe200 and MFe300 samples. They were obtained with the purpose of detecting changes in oxidation, according to the chemical equation:

$$Fe_3O_4 + O_2 \rightarrow Fe_2O_3 \cdot Fe_3O_4$$

Figures 5b–e show high-resolution spectra and deconvolution into six peaks of MFe, MFe100, MF200 and MFe300 samples. Fe 2p high resolution spectrum is composed of two spectral bands located at 725.3 eV, and 711.9 eV, corresponding to $2p_{1/2}$, and $2p_{3/2}$ of Fe^{3+} species, respectively. Also, the other two peaks at a binding energy of 723.8 eV and 710.6 eV are attributed to $2p_{1/2}$ and $2p_{3/2}$ of the Fe^{2+} species, respectively. The remaining two weak peaks at 719 eV and 733 eV are satellite peaks. These results and assignments agree with reports of other authors for Fe_3O_4 and Fe_2O_3 samples, indicating the successful formation of iron oxide compounds in the mordenite matrix [51–53]. Table 2 presents oxidation states of deconvolution estimates of species present in studied samples. They were calculated through the integral of deconvoluted signals in individual XPS peaks. Fe^{3+} peak signal increases with temperature treatment, from 46 At% to 55 At%, which could be related to an oxidation process. At the same time, the Fe^{2+} peak signal decreases with temperature treatment, from 54 At% to 45 At%. Then, because of thermal treatment, Fe^{2+} in Fe_3O_4 partially becomes Fe^{3+} in Fe_2O_3 in studied samples, allowing to obtain Fe_2O_3 and

Table 2 Atomic percent oxidation states of iron oxide species in Fe_3O_4–Fe_2O_3 supported on mordenite samples as a function of temperature in oxidative thermal treatment

Fe_3O_4–Fe_2O_3 supported on mordenite samples	At% Fe^{2+}	At% Fe^{3+}
MFe	54	46
MFe100	48	52
MFe200	47	53
MFe300	45	55

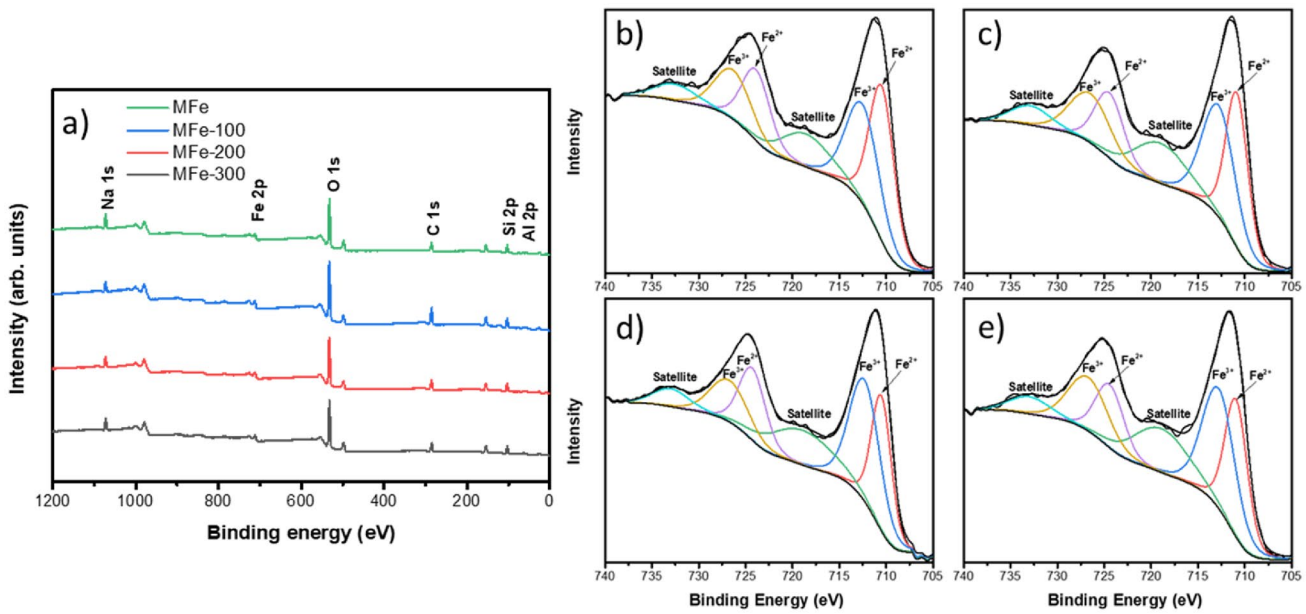

Fig. 5 **a** XPS full Survey spectra of Fe_3O_4–Fe_2O_3 supported on mordenite samples and deconvolution of high-resolution XPS spectra of Fe 2p **b** MFe, **c** MFe100, **d** MFe200 and **e** MFe300 samples

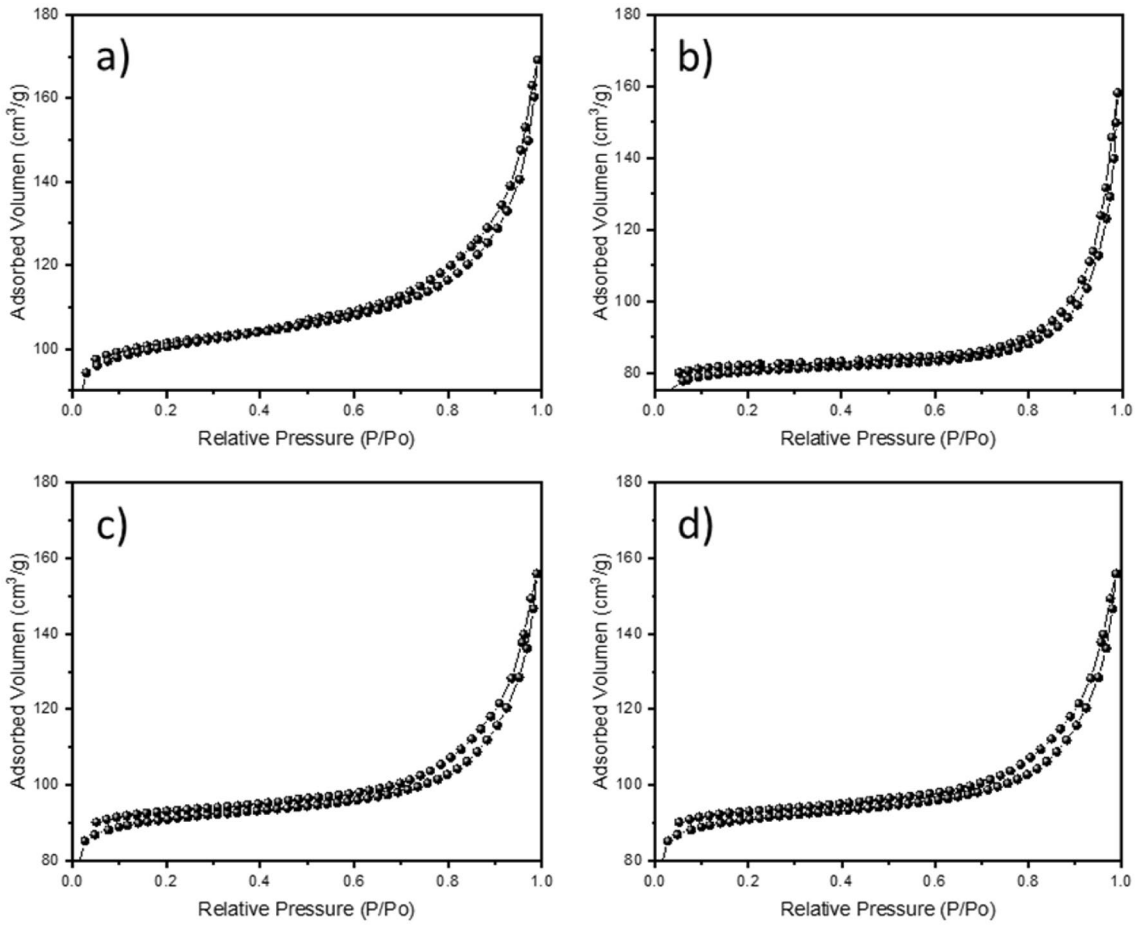

Fig. 6 Pore size distribution Adsorption–desorption profile of **a** MFe, **b** MFe100, **c** MFe200, **d** MFe300 samples

Table 3 Textural parameters of Fe_3O_4–Fe_2O_3 supported on mordenite samples

Catalyst	S_{BET} (cm^2/g)	V_{pore} (cm^3/g)	D_{pore} (nm)
MFe	296	0.06	4.6
MFe100	290	0.06	4.7
MFe200	274	0.05	4.9
MFe300	267	0.05	5.0

Fe_3O_4 in different relative concentrations in the same sample through a simple oxidative thermal process.

4.5 Surface area analysis

Figure 6 shows results of N_2 adsorption–desorption isotherms of (a) MFe, (b) MFe100, (c) MFe200, (d) MFe300 samples. They exhibit low adsorption at low relative pressure and hysteresis characteristic of interparticle mesopores of the aggregates present in zeolites [54–56]. Table 3 shows textural parameters of the synthesized catalysts. Adsorbed amount of nitrogen, represented by S_{BET}, slowly decreases with thermal treatment temperature, which could be due to sintering and/or dealumination. Volume and diameter of pore show little change within the uncertainty of measurement. A similar effect was observed in previous work with hydrotreated Cu-Ag/mordenite catalysts for NO reduction [57]. The textural properties are related to organic compounds adsorption application and its possible elimination for the remediation process, due to the surface area of the catalyst interacting with organic dye pollution via electrostatic forces. Moreover, the pore of the catalyst is related to the active catalytic centers where dye will be degraded by the photocatalysis and fenton process [58, 59].

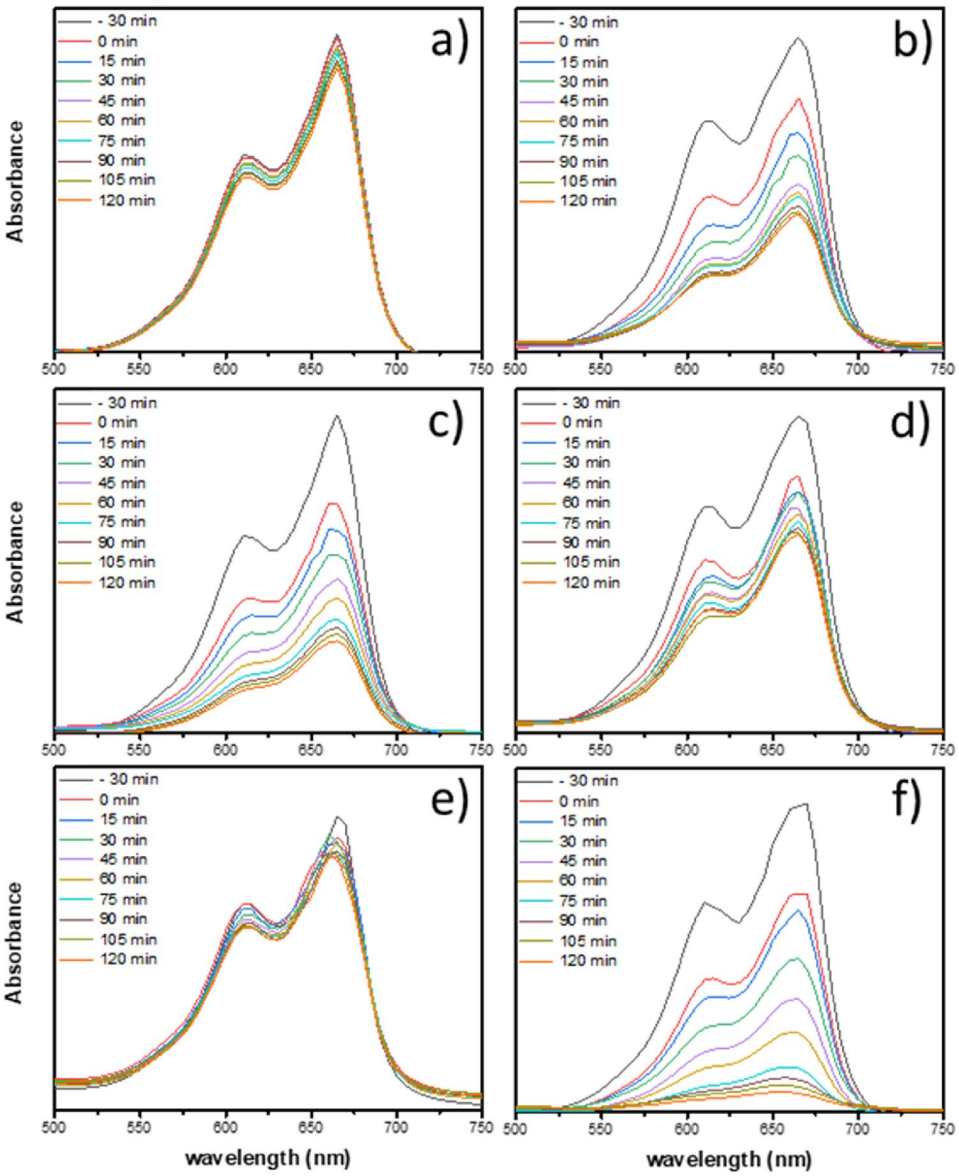

Fig. 7 UV–visible absorption spectra of photodegradation of MB with visible light excitation for 120 min with previous agitation in dark condition (– 30 min to 0 min) of catalysts of **a** M, **b** MFe, **c** MFe100, **d** MFe200, **e** MFe300 and **f** MFe100 together with H_2O_2

4.6 Photocatalytic MB degradation

Photocatalytic methylene blue (MB) degradation by the catalysts synthesized was evaluated with visible light excitation. Figure 7 presents the results of UV–visible absorption spectra after photodegradation of MB with visible light for different times of (a) M, (b) MFe, (c) MFe100, (d) MFe200 and (e) MFe300; and (f) MFe100 together with H_2O_2. Studied catalysts with iron oxides present different decrements in absorbance as function of time, indicating MB degradation with visible light exposition. Absorbance curves show an important contribution from the adsorption effects of MB in the dark (black line, – 30 min) before visible light irradiation exposure on Fe_3O_4–Fe_2O_3 supported on mordenite which is the typical behavior in synthetic zeolites with a high Si/Al ratio and could be due to organic residues adsorbed. Figure 8a exhibits results of relative photocatalytic efficiency, represented by C/Co as a function of time of exposure, and Fig. 8b shows kinetics of photocatalytic degradation of MB with visible light of studied catalysts, pristine mordenite and Fe_3O_4–Fe_2O_3 supported on mordenite samples. MFe100 shows the best photocatalytic activity with almost 70% MB degradation after 120 min, without adding a co-catalyst (Fig. 8a). The Fenton effect was proved by adding 2.5 ml of H_2O_2 to MFe100 sample during the MB photocatalytic degradation [60, 61]. Figures 8a and b show how adding H_2O_2 improves photocatalytic efficiency and kinetics of photocatalytic degradation of MB with visible light, reaching ~ 90% MB degradation after 120 min. On the other hand, M and MFe300 samples do not present

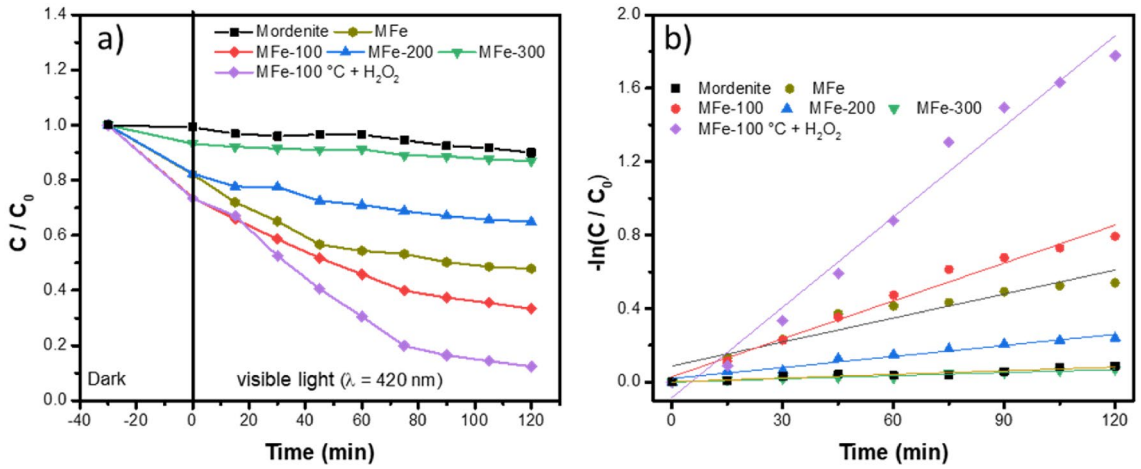

Fig. 8 **a** The relative photocatalytic efficiency (C/C_o) as function of reaction time (t) and **b** kinetics of photocatalytic degradation of MB with visible light of mordenite pristine and Fe_3O_4–Fe_2O_3 supported on mordenite as a function of reaction time (t) in logarithmic scale [$-ln(C/Co)$], and matched straight lines to first-order reaction kinetics

Table 4 Kinetic constants of MB photodegradation of Fe_3O_4–Fe_2O_3 supported on mordenite samples

Catalyst	% MB degradation	R^2	k (min^{-1})
MFe	53	0.91	4.3×10^{-3}
MFe100	70	0.98	6.9×10^{-3}
MFe200	36	0.97	2.0×10^{-3}
MFe300	14	0.96	5.7×10^{-4}
MFe100 + H_2O_2	90	0.98	1.6×10^{-2}
M	9	0.95	6.67×10^{-4}

considerable photocatalytic activity. Therefore, increasing the temperature of the thermal treatment slightly favored more oxidation in the samples, according to XPS results, increasing Fe_2O_3 concentration in comparison with Fe_3O_4, also modification of the surface area, crystallinity and morphology, which could be related with properties for photocatalytic applications.

Curves of relative concentration as a function of time based on the first order kinetic reaction equation [62, 63] was matched to study the kinetics of MB photodegradation, according to the equation:

$$-ln\frac{C}{C_0} = kt$$

where C_0 and C are respective initial and real-time MB concentrations, and k is the first-order degradation rate constant with visible light. Matched lines are shown in Fig. 8b, and obtained kinetic constants are described in Table 4. Rate constant increases from 0.0043 to 0.0069 min^{-1} from MFe samples to MFe100 corresponding to ~ 60% increase.

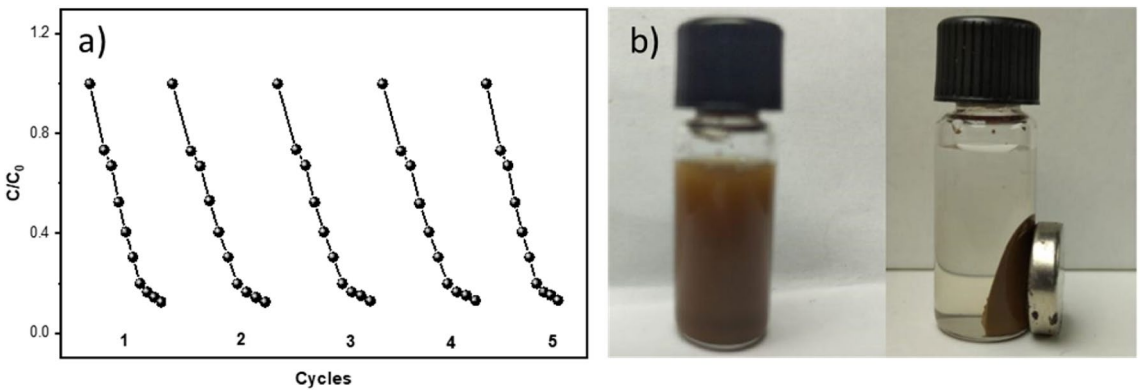

Fig. 9 **a** Photocatalytic stability test to five cycles of MFe100 and **b** magnetic retrieval with a permanent magnet of MFe100 sample

Also, rate constant increases about four times from 0.0043 to 0.016 min^{-1} after MFe100 and a small portion of hydrogen peroxide addition on the Fe_3O_4–Fe_2O_3 supported on mordenite catalysts. Considering the rate constant reaction of MB degradation of this catalyst, an extrapolation indicates it could eliminate 99%, approximately, after 180 min of visible irradiation.

Stability of the catalyst was investigated by monitoring the catalytic activity during successive cycles of degradation and results are shown in Fig. 9a, where C_0 and C are the initial and real-time MB concentrations, respectively. MFe100 exhibits a very stable photocatalytic performance after five cycles of test without significant loss of activity. Additionally, Fig. 9b shows one of the synthesized catalysts with iron oxides before and after bringing closer a magnet, indicating clearly that thanks to the magnetic properties of the synthesized catalysts it is possible to recover the catalyst through a magnetic field, allowing its reusability in applications of wastewater photodegradation.

4.7 Mechanism of MB degradation

A possible main mechanism for degradation of MB in Fe_3O_4–Fe_2O_3/mordenite + H_2O_2 + Visible light system proposed is: (1) MB is adsorbed in the mordenite support pores through electrostatic interaction, (2) $HO^{\bullet}$ radicals produced by H_2O_2 activated with photo oxide of Fe^{2+} and $HOO^{\bullet}$ radicals produced by H_2O_2 activated with photoreduced of Fe^{3+} on the surface of Fe_3O_4–Fe_2O_3 supported on mordenite samples; and simultaneous process (3) photocatalysis with visible light photons to photogenerated electron–hole pairs that reduces and oxidizes, respectively, O_2 and H_2O present, generated reactive species $OO^{\bullet}$ and $HO^{\bullet}$, (4) adsorbed MB in Fe_3O_4–Fe_2O_3 supported on mordenite sample is attacked by $HO^{\bullet}$, $OO^{\bullet}$, and $HOO^{\bullet}$, produced by Fenton reaction and photocatalyst. Active centers of MB around the catalyst are provided by the mordenite support with a large surface area. Incorporation of Fe_3O_4–Fe_2O_3 particles on mordenite seems to greatly enhance the transformation from Fe^{3+} to Fe^{2+} or the recycling of iron species [64, 65]. This possible photocatalytic mechanism of Fe_3O_4–Fe_2O_3 supported on mordenite for MB degradation is depicted in Fig. 10.

5 Conclusions

A set of Fe_3O_4–Fe_2O_3 supported on mordenite catalysts with different thermal treatments was successfully synthesized by using a simple chemical method and its physicochemical properties were confirmed by DRX, SEM, EDS, XPS, S_{BET}, UV–Vis DR. Crystalline structure and morphology of studied samples are related to thermal treatment. Due to the presence of iron oxides, catalyst samples synthesized with iron oxides have more visible light absorption than pristine mordenite. Samples have a significant temperature dependence with crystallinity, particle agglomeration, surface area, and other textural properties. Sample MFe100 presented the best

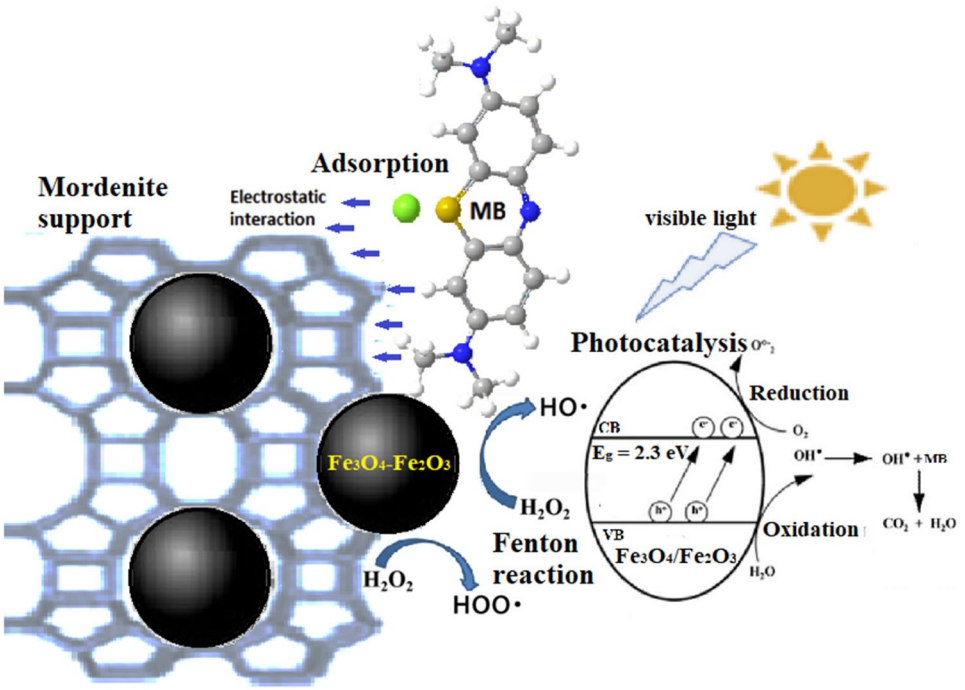

Fig. 10 Catalytic oxidation mechanism of MB in Fe_3O_4–Fe_2O_3 supported on mordenite + H_2O_2 + Visible light system

photodegradation capabilities with visible light excitation. This behavior could be attributed to methylene blue degradation by three processes: adsorption of organic residues in the mordenite matrix support due to electrostatic interactions, photocatalysis heterogeneous reaction with visible light and Fenton reaction catalyst with a small portion of H_2O_2 by presence of Fe_3O_4–Fe_2O_3. Due to the magnetic properties of the Fe_3O_4–Fe_2O_3 supported on mordenite samples the catalyst could be retrieved and reused in the photodegradation process. Obtained catalyst MFe100 was able to degrade MB ~ 90% after 120 min. The catalysts synthesized with the presence of Fe_3O_4–Fe_2O_3 using visible light for MB degradation were prepared following simple and economical thermal treatments without changing pH, temperature, dose or other conditions. Additionally, catalysts can be retrieved and reused at least five times by using a magnetic field. These catalysts could be proposed for the remediation of wastewater using visible light or solar excitation related to textile, food and pharmaceutical industries.

Acknowledgements This work was supported by DGAPA–UNAM research project PAPIIT IN111622, and CONAHCyT through the FORDECyT project 272894, SENER-CONAHCyT- 117373 and Basic Scientific Research A1-S-26789 and A1-S-17539. RAM thanks CONAHCYT Estancias Postdoctorales por México program, project 3241760, for financial support of this work. The authors would like to thank L. Arce, D. Domínguez, F. Ruiz, J. Mendoza, J. A. Diaz, I. Gradilla, E. Murillo, and E. Aparicio for their valuable technical assistance.

Author contributions RA-M: writing—original draft, visualization, methodology, validation, investigation, formal analysis, data curation, conceptualization. HABN: writing—review & editing, writing—original draft, visualization, validation, methodology, investigation, formal analysis, conceptualization. MHF: writing—review & editing. FC-B: investigation, funding acquisition, formal analysis, conceptualization, methodology, writing—original draft.

Funding DGAPA–UNAM, PAPIIT IN111622, Consejo Nacional de Humanidades, Ciencias y Tecnologías, CONAHCYT-FORDECyT project 272894

Declarations

Conflict of interest The authors declare that they have no known competing financial interests or personal relationships that could have appeared to influence the work reported in this paper.

Data availability Data will be made available on request.

Code availability Not Applicable.

Ethical approval Not Applicable.

References

1. Wang X, Jiang J, Gao W (2022) Reviewing textile wastewater produced by industries: characteristics, environmental impacts, and treatment strategies. Water Sci Technol 85:2076–2096. https://doi.org/10.2166/wst.2022.088
2. Anwer H, Mahmood A, Lee J et al (2019) Photocatalysts for degradation of dyes in industrial effluents: opportunities and challenges. Nano Res 12:955–972. https://doi.org/10.1007/s12274-019-2287-0
3. Tkaczyk A, Mitrowska K, Posyniak A (2020) Synthetic organic dyes as contaminants of the aquatic environment and their implications for ecosystems: a review. Sci Total Environ 717:137222. https://doi.org/10.1016/j.scitotenv.2020.137222
4. Shanker U, Rani M, Jassal V (2017) Degradation of hazardous organic dyes in water by nanomaterials. Environ Chem Lett 15:623–642. https://doi.org/10.1007/s10311-017-0650-2
5. Rafiq A, Ikram M, Ali S et al (2021) Photocatalytic degradation of dyes using semiconductor photocatalysts to clean industrial water pollution. J Ind Eng Chem 97:111–128. https://doi.org/10.1016/j.jiec.2021.02.017
6. Viswanathan B (2017) Photocatalytic degradation of dyes: an overview. Curr Catal 7:99–121. https://doi.org/10.2174/2211544707666171219161846
7. Pirsaheb M, Hossaini H, Raad NK et al (2023) A systematic review on photo-Fenton process as an efficient advanced oxidation for degradation of amoxicillin in aqueous environments. Rev Environ Health 38:313–326. https://doi.org/10.1515/reveh-2021-0155
8. Din MI, Khalid R, Najeeb J, Hussain Z (2021) Fundamentals and photocatalysis of methylene blue dye using various nanocatalytic assemblies- a critical review. J Clean Prod 298:1236567. https://doi.org/10.1016/j.jclepro.2021.126567
9. Mussa ZH, Al-Ameer LR, Al-Qaim FF et al (2023) A comprehensive review on adsorption of methylene blue dye using leaf waste as a bio-sorbent: isotherm adsorption, kinetics, and thermodynamics studies. Environ Monit Assess. https://doi.org/10.1007/s10661-023-11432-1
10. Oladoye PO, Ajiboye TO, Omotola EO, Oyewola OJ (2022) Methylene blue dye: toxicity and potential elimination technology from wastewater. Res Eng 16:100678. https://doi.org/10.1016/j.rineng.2022.100678
11. Saeed M, Muneer M, Ul Haq A, Akram N (2022) Photocatalysis: an effective tool for photodegradation of dyes-a review. Environ Sci Pollut Res 29:293–311. https://doi.org/10.1007/s11356-021-16389-7/Published
12. Dong S, Feng J, Fan M et al (2015) Recent developments in heterogeneous photocatalytic water treatment using visible light-responsive photocatalysts: a review. RSC Adv 5:14610–14630. https://doi.org/10.1039/C4RA13734E
13. Al-Jemeli M, Mahmoud MA, Majdi HS et al (2021) Degradation of anti-inflammatory drugs in synthetic wastewater by solar

photocatalysis. Catalysts 11:1330. https://doi.org/10.3390/catal11111330
14. Bassim S, Mageed AK, AbdulRazak AA, Al-Sheik F (2023) Photodegradation of methylene blue with aid of green synthesis of CuO/TiO_2 nanoparticles from extract of citrus aurantium juice. Bullet Chem React Eng Catal 18:1–16. https://doi.org/10.9767/bcrec.16417
15. Xin Y, Zhu Q, Gao T et al (2023) Photocatalytic NO removal over defective Bi/BiOBr nanoflowers: the inhibition of toxic NO_2 intermediate via high humidity. Appl Catal B 324:122238. https://doi.org/10.1016/j.apcatb.2022.122238
16. Dawi EA, Padervand M, Ghasemi S et al (2023) Multi-functional fluorinated NiTiO3 perovskites for CO_2 photocatalytic reduction, electrocatalytic water splitting, and biomedical waste management. J Water Process Eng 54:2214-7144. https://doi.org/10.1016/j.jwpe.2023.103979
17. Hitam CNC, Jalil AA (2020) A review on exploration of Fe_2O_3 photocatalyst towards degradation of dyes and organic contaminants. J Environ Manage 258:110050. https://doi.org/10.1016/j.jenvman.2019.110050
18. Campos EA, Pinto DVBS, de Oliveira JIS et al (2015) Synthesis, characterization and applications of iron oxide nanoparticles—A short review. J Aerosp Technol Manag 7:267–276. https://doi.org/10.5028/jatm.v7i3.471
19. Bhateria R, Singh R (2019) A review on nanotechnological application of magnetic iron oxides for heavy metal removal. J Water Process Eng 31:100845. https://doi.org/10.1016/j.jwpe.2019.100845
20. Malhotra N, Lee JS, Liman RAD et al (2020) Potential toxicity of iron oxide magnetic nanoparticles: a review. Molecules 25:3159. https://doi.org/10.3390/molecules25143159
21. Hasany SF, Ahmed I, Rajan J, Rehman A (2013) Systematic review of the preparation techniques of iron oxide magnetic nanoparticles. Nanosci Nanotechnol 2:148–158. https://doi.org/10.5923/j.nn.20120206.01
22. Sangaiya P, Jayaprakash R (2018) A review on iron oxide nanoparticles and their biomedical applications. J Supercond Nov Magn 31:3397–3413
23. Wei X, Xie T, Peng L et al (2011) Effect of heterojunction on the behavior of photogenerated charges in Fe_3O_4@Fe_2O_3 nanoparticle photocatalysts. J Phys Chem C 115:8637–8642. https://doi.org/10.1021/jp111250z
24. Li N, He Y, long, Yi Z zhou, et al (2020) Multiple-metal-doped Fe_3O_4@Fe_2O_3 nanoparticles with enhanced photocatalytic performance for methyl orange degradation under UV/solar light irradiation. Ceram Int 46:19038–19045. https://doi.org/10.1016/j.ceramint.2020.04.234
25. Palanisamy B, Babu CM, Sundaravel B et al (2013) Sol-gel synthesis of mesoporous mixed Fe_2O_3/TiO_2 photocatalyst: Application for degradation of 4-chlorophenol. J Hazard Mater 252–253:233–242. https://doi.org/10.1016/j.jhazmat.2013.02.060
26. Padervand M, Rhimi B, Wang C (2021) One-pot synthesis of novel ternary Fe_3N/Fe_2O_3/C_3N_4 photocatalyst for efficient removal of rhodamine B and CO_2 reduction. J Alloys Compd 825:156955. https://doi.org/10.1016/j.jallcom.2020.156955
27. Crini G, Lichtfouse E, Wilson LD, Morin-Crini N (2019) Conventional and non-conventional adsorbents for wastewater treatment. Environ Chem Lett 17:195–213. https://doi.org/10.1007/s10311-018-0786-8
28. Rangnekar N, Mittal N, Elyassi B et al (2015) Zeolite membranes—a review and comparison with MOFs. Chem Soc Rev 44:7128–7154. https://doi.org/10.1039/C5CS00292C
29. Van Speybroeck V, Hemelsoet K, Joos L et al (2015) Advances in theory and their application within the field of zeolite chemistry. Chem Soc Rev 44:7044–7111. https://doi.org/10.1039/C5CS00029G
30. Król M (2020) Natural vs synthetic zeolites. Crystals (Basel) 10:1–8. https://doi.org/10.3390/cryst10070622
31. Kalvachev Y, Todorova T, Popov C (2021) Recent progress in synthesis and application of nanosized and hierarchical mordenite—a short review. Catalysts 11:1–16. https://doi.org/10.3390/catal11030308
32. Narayanan S, Tamizhdurai P, Mangesh VL et al (2020) Recent advances in the synthesis and applications of mordenite zeolite - review. RSC Adv 11:250–267. https://doi.org/10.1039/D0RA09434J
33. Jorfi S, Pourfadakari S, Kakavandi B (2018) A new approach in sono-photocatalytic degradation of recalcitrant textile wastewater using MgO@Zeolite nanostructure under UVA irradiation. Chem Eng J 343:95–107. https://doi.org/10.1016/j.cej.2018.02.067
34. Rahmani-Aliabadi A, Nezamzadeh-Ejhieh A (2018) A visible light FeS/Fe_2S_3/zeolite photocatalyst towards photodegradation of ciprofloxacin. J Photochem Photobiol A Chem 357:1–10. https://doi.org/10.1016/j.jphotochem.2018.02.006
35. Padervand M, Heidarpour H, Bargahi A (2020) A mechanistic study and in-vivo toxicity bioassay on acetamiprid photodegradation over the zeolite supported cerium-based photocatalyst. J Photochem Photobiol A Chem 395:112526. https://doi.org/10.1016/j.jphotochem.2020.112526
36. Torkian N, Bahrami A, Hosseini-Abari A et al (2022) Synthesis and characterization of Ag-ion-exchanged zeolite/TiO_2 nanocomposites for antibacterial applications and photocatalytic degradation of antibiotics. Environ Res 207:112157. https://doi.org/10.1016/j.envres.2021.112157
37. Liu J, Lin H, Dong Y et al (2022) MoS_2 nanosheets loaded on collapsed structure zeolite as a hydrophilic and efficient photocatalyst for tetracycline degradation and synergistic mechanism. Chemosphere 287:132211. https://doi.org/10.1016/j.chemosphere.2021.132211
38. Besenhard MO, LaGrow AP, Hodzic A et al (2020) Co-precipitation synthesis of stable iron oxide nanoparticles with NaOH: New insights and continuous production via flow chemistry. Chem Eng J 399:125740. https://doi.org/10.1016/j.cej.2020.125740
39. Hariani PL, Faizal M, Ridwan R et al (2013) Synthesis and properties of Fe_3O_4 nanoparticles by Co-precipitation method to removal procion dye. Int J Environ Sci Develop 4:336. https://doi.org/10.7763/ijesd.2013.v4.366
40. Radoń A, Drygała A, Hawełek Ł, Łukowiec D (2017) Structure and optical properties of Fe_3O_4 nanoparticles synthesized by co-precipitation method with different organic modifiers. Mater Charact 131:148–156. https://doi.org/10.1016/j.matchar.2017.06.034
41. Anbarasu M, Anandan M, Chinnasamy E et al (2015) Synthesis and characterization of polyethylene glycol (PEG) coated Fe_3O_4 nanoparticles by chemical co-precipitation method for biomedical applications. Spectrochim Acta A Mol Biomol Spectrosc 135:536–539. https://doi.org/10.1016/j.saa.2014.07.059
42. Kandpal ND, Sah N, Loshali R, et al. (2014) Co-precipitation method of synthesis and characterization of iron oxide nanoparticles. J Sci Ind Res 73:87-90.
43. Ahmed FS, AbdulRazak AA, Alsaffar MA (2022) Modelling and optimization of methylene blue adsorption from wastewater utilizing magnetic marble dust adsorbent: a response surface methodology approach. Mater Today Proc 60:1676–1688. https://doi.org/10.1016/j.matpr.2021.12.224
44. Gao Q, Chen F, Zhang J et al (2009) The study of novel Fe_3O_4@γ-Fe_2O_3 core/shell nanomaterials with improved properties. J Magn Magn Mater 321:1052–1057. https://doi.org/10.1016/j.jmmm.2008.10.022

45. Gallagher KJ, Feitknecht W, Mannweiler U (1968) Mechanism of oxidation of magnetite to y-Fe_2O_3. Nature 217:1118–1121. https://doi.org/10.1038/2171118a0
46. Kang YS, Risbud S, Rabolt JF, Stroeve P (1996) Synthesis and characterization of nanometer-size Fe_3O_4 and γ-Fe_2O_3 particles. Chem Mater 8:2209–2211. https://doi.org/10.1021/cm960157j
47. Shao Q, Wei S, Hu X, Dong H, Wen T, Gao L, Long C (2022) Tuning the micro-coordination environment of Al in dealumination Y zeolite to enhance electron transfer at the Cu-Mn oxides interface for highly efficient catalytic ozonation of toluene at low temperatures. Environ Sci Technol 56(22):15449–15459. https://doi.org/10.1021/acs.est.2c05766
48. Tauc J, Grigorovici R, Vancu A (1966) Optical properties and electronic structure of Ge optical properties and electronic structure of amorphous germanium. Physica Status Solidi (b) 15:627. https://doi.org/10.1002/pssb.19660150224
49. Aydn C, Abd El-Sadek MS, Zheng K et al (2013) Synthesis, diffused reflectance and electrical properties of nanocrystalline Fe-doped ZnO via sol-gel calcination technique. Opt Laser Technol 48:447–452. https://doi.org/10.1016/j.optlastec.2012.11.004
50. Kulkarni SA, Sawadh PS, Palei PK, Kokate KK (2014) Effect of synthesis route on the structural, optical and magnetic properties of Fe_3O_4 nanoparticles. Ceram Int 40:1945–1949. https://doi.org/10.1016/j.ceramint.2013.07.103
51. Tahir D, Ilyas S, Abdullah B et al (2018) Electronic properties of composite iron (II, III) oxide (Fe_3O_4) carbonaceous absorber materials by electron spectroscopy. J Electron Spectros Relat Phenomena 229:47–51. https://doi.org/10.1016/j.elspec.2018.09.008
52. Liu HL, Wu JH, Min JH et al (2009) Monosized core-shell Fe_3O_4(Fe)/Au multifunctional nanocrystals. J Nanosci Nanotechnol 9(2):754–758. https://doi.org/10.1166/jnn.2009.c018
53. Wilson D, Langell MA (2014) XPS analysis of oleylamine/oleic acid capped Fe_3O_4 nanoparticles as a function of temperature. Appl Surf Sci 303:6–13. https://doi.org/10.1016/j.apsusc.2014.02.006
54. Huang S, Chen P, Yan B et al (2013) Modification of y zeolite with alkaline treatment: textural properties and catalytic activity for diethyl carbonate synthesis. Ind Eng Chem Res 52:6349–6356. https://doi.org/10.1021/ie3032235
55. Triantafyllidis KS, Karakoulia SA, Gournis D et al (2008) Formation of carbon nanotubes on iron/cobalt oxides supported on zeolite-Y: Effect of zeolite textural properties and particle morphology. Microporous Mesoporous Mater 110:128–140. https://doi.org/10.1016/j.micromeso.2007.10.007
56. Aguado J, Serrano DP, Escola JM, Peral A (2009) Catalytic cracking of polyethylene over zeolite mordenite with enhanced textural properties. J Anal Appl Pyrolysis 85:352–358. https://doi.org/10.1016/j.jaap.2008.10.009
57. Ramírez-Garza RE, Rodríguez-Iznaga I, Simakov A, Farías MH, Castillón-Barraza FF (2018) Cu-Ag/mordenite catalysts for NO reduction: effect of silver on catalytic activity and hydrothermal stability. Mater Res Bull 97:369–378. https://doi.org/10.1016/j.materresbull.2017.09.001
58. Harja M, Buema G, Bucur D (2022) Recent advances in removal of Congo Red dye by adsorption using an industrial waste. Sci Rep 12:6087. https://doi.org/10.1038/s41598-022-10093-3
59. Afroze S, Sen TK (2018) A review on heavy metal ions and dye adsorption from water by agricultural solid waste adsorbents. Water Air Soil Pollut 229: 225. https://doi.org/10.1007/s11270-018-3869-z
60. Clarizia L, Russo D, di Somma I et al (2017) Homogeneous photo-Fenton processes at near neutral pH: a review. Appl Catal B 209:358–371. https://doi.org/10.1016/j.apcatb.2017.03.011
61. Ameta R, Chohadia AK, Jain A, Punjabi PB (2018) Fenton and Photo-Fenton Processes. Advanced Oxidation Processes for Wastewater Treatment: Emerging Green Chemical Technology. Elsevier, Amsterdam, pp 49–87. https://doi.org/10.1016/B978-0-12-810499-6.00003-6
62. Konstantinou IK, Albanis TA (2004) TiO_2-assisted photocatalytic degradation of azo dyes in aqueous solution: Kinetic and mechanistic investigations: a review. Appl Catal B 49:1–14. https://doi.org/10.1016/j.apcatb.2003.11.010
63. Mahmoodi NM, Arami M, Limaee NY, Tabrizi NS (2006) Kinetics of heterogeneous photocatalytic degradation of reactive dyes in an immobilized TiO_2 photocatalytic reactor. J Colloid Interface Sci 295:159–164. https://doi.org/10.1016/j.jcis.2005.08.007
64. Khan I, Saeed K, Zekker I, Zhang B, Hendi AH, Ahmad A, Ahmad S, Zada N, Ahmad H, Shah LA (2022) Review on Methylene blue: its properties, uses. Toxic Photodegradation. Water 14(2):242. https://doi.org/10.3390/w14020242
65. Wang Q, Tian S, Ningv P (2014) Degradation mechanism of methylene blue in a heterogeneous fenton-like reaction catalyzed by ferrocene. Ind Eng Chem Res 53(2):643–649. https://doi.org/10.1021/ie403402q